Numerical and experimental methodology for the development of a new membrane prototype intended to microfiltration bioprocesses. Application to milk filtration

Fanny Springer, Emilie Carretier, D. Veyret, D. Dhaler, Philippe Moulin

Numerical and experimental methodology for the development of a new membrane prototype intended to microfiltration bioprocesses. Application to milk filtration

F. Springer [a], E. Carretier [a], D. Veyret [b], D. Dhaler [c], P. Moulin [a,*]

a Université Paul Cézanne Aix Marseille, Laboratoire de Mécanique, Modélisation et Procédés Propres (M2P2–CNRS-UMR 6181), Europôle de l'Arbois, 13545 Aix en Provence, France
b European Commission, DG JRC-IE, NL-1755 LE Petten, Netherlands
c Novasep Applexion SAS, Site St Maurice de Beynost, 5, Chemin du Pilon, 01708 Miribel, France

In tangential flow filtration, the non-uniform TransMembrane Pressure (TMP) on the membrane length produces a non homogeneous filtration cake, initiates process selectivity changes and modifies the permeate quality. The purpose of this study is to create a tubular ceramic membrane prototype with a more uniform TMP, intended to filtration of fouling fluids. The principle of this membrane structure is to waterproof the external membrane surface to limit flow circulation in the porous support of the membrane. The production was controlled by sizing «permeation vents». This development was achieved using a CFD modelling tool interacting with experiments. A preliminary modelling study was made with water. This work was afterwards applied to the industrial process of casein micelle separation from skim milk. The influence of operating conditions on the membrane hydrodynamics was highlighted. The modelling results were experimentally confirmed, with a discrepancy smaller than 3% and a reproducible water permeability of 2.3 L h^{-1} bar^{-1} for 1 mm-wide vent (TMP = 1 bar, T = 20 °C). Then, milk filtration experiments showed a production ratio milk/water equal to 1/2. The permeate quality parameters were studied and the fouling phenomena were taken into account. A parametric study led to the sizing of a final prototype. Its efficiency was experimentally evaluated.

1. Introduction

Though the concept of membrane filtration process is simple, phenomena linked to mechanical and physico-chemical interactions between the membrane and the fluid remain complex. The first phenomenon observed is the flux decline with filtration time, due to the concentration polarisation and fouling deposit. Those phenomena tend to modify the selectivity performance of the filtration process with a consequent modification of the collected retentate and permeate quality. The alteration of filtration efficiency is also linked to TMP (TransMembrane Pressure). The higher the TMP, the more the permeate flow circulation observed at the first filtration instants. Thus, fouling build up occurs more rapidly and the filtration cake formed is more compressed. In the case of a tangential fluid flow filtration, the TMP and the deposit on the membrane surface can be highly heterogeneous on the monolith length [1]. Consequently, the retention characteristics are not constant along the membrane length. Those phenomena are accentuated with the complexity and the concentration of the filtered fluids. In particular, it is often the case for the fluids treated in food-bioprocess industry. In this field, the use of membrane filtration has been widely spread for beverage treatment, animal and valuable vegetal proteins recovery.

It was pointed out that the pore blocking mechanism was predominant in the case of microfiltration membranes [2]. Considering Bovine Serum Albumin (BSA) filtration, Chen highlighted fouling mechanisms in microfiltration [3]. The initial deposit of proteins is the trigger to the global formation of fouling and it controls the nature of the secondary dynamic membrane. For instance, the charge of the first proteins deposited on the membrane surface modifies the chemical properties of the surface, the charge distribution, the hydrophobic and receptiveness of the surface for a subsequent deposition. Le Berre and Daufin observed the filtration cake characteristics and the evolution of performance with time in milk microfiltration process [4]. In the case of short filtration times, the fouling cake was not formed tightly; its porosity let the smallest micelles permeate. With time, the erosion due to wall shear stress blew the biggest particles off and left the smallest in the filtration cake structure. The cake filtration porosity decreased and caused an increasing global resistance of the structure and a decreasing trans-

* Corresponding author.
E-mail address: philippe.moulin@univ-cezanne.fr (P. Moulin).

mission of soluble proteins. Wenten added to those phenomena the effect of the local shear stress. The blocked proteins at the membrane pore entrance may be altered by a high local shear stress [5]. Once this alteration was initiated, the microfiltration membrane transmitted less proteins and behaved rather as an ultrafiltration membrane. The link between the structure of the filtration cake and the permeate quality was clearly demonstrated, which requires to limit and control fouling.

Several technical solutions were implemented and empirically established. They can be simultaneously applied and bring improvement to the process, without being an ultimate solution. With the purpose of increasing turbulence at the membrane surface, the VSEP (Vibratory Shear Enhanced Process) concept, rotating disk modules [6], microvibrations [7], Dean vortices formation [8], insertion of spacers or flexible suspended carriers inside filtration modules were used in industry. The concept of new processes specifically adapted or geometrically modified to reduce fouling generated by filtration process is commonly spread [9]. Nevertheless, as reported in literature, increasing flow turbulence using mechanical means is not sufficient to improve microfiltration process.

Chen reported that controlling the initial protein deposit may potentially reduce the filtration cake thickness [3]. Monitoring starting parameters such as TMP, wall concentration or flux are determining factors for the process run. However, those methods remain empirical. Since the operating conditions of the filtration are crucial for fouling formation and accumulation, studying the influence of the process parameters on the fouling characteristics finally appears as the most relevant methodology.

1.1. Shear stress and tangential fluid flow

The shear stress is a significant hydrodynamic parameter characterizing the mass transfer at the membrane surface. Gésan-Guiziou et al. [10] and later Mercier-Bonin et al. [1] investigated the influence of the shear stress in the case of a gas/liquid fluid flow applied to skimmed milk microfiltration with a 0.1 μm membrane nominal pore size. Later, the effect of the shear stress on membrane filtration performance during milk microfiltration and ultrafiltration were demonstrated [11,12]. The tangential fluid flow is a dominant factor, controlling the deposit and the filtration cake erosion [13].

Performance of skim milk microfiltration depended on the permeate flux and the wall shear stress [4]. Thus, it was possible to define critical operating conditions. The critical ratio permeate flux/wall shear stress (J/τ_w) characterized the transition to irreversible deposition by expressing the balance between convective forces – induced by the mass transfer at the membrane surface – and the drag forces – induced by the shear stress which prevents the build-up of cake and alters the solidity of the wall deposit. Exceeding the critical value of this empirically established ratio caused particles dragging toward the membrane wall. Rapid accumulation of the milk components at the membrane surface led to irreversible modifications of the deposit characteristics [14,15]. Inversely, maintaining this ratio under the critical zone permitted sustainable process performance. Gésan-Guiziou et al. established the critical value of this parameter [10] in the case of 0.1 μm microfiltration with a multichannel Kerasep™ ceramic membrane:

$$\frac{J}{\tau_w} = 0.95 \ \text{L h}^{-1} \ \text{m}^{-2} \ \text{Pa}^{-1} \quad (1)$$

This critical ratio was demonstrated accurate in most filtration process studies. Nevertheless, some exceptions were brought into evidence [16]. Furthermore, even if the wall shear stress was highly increased and allowed a considerable gain of permeate flux, protein transmission may be affected and decreased [4].

1.1.1. Wall concentration

Arguing that the duration of the filtration cycles and the protein selectivity depend on the same factor of concentration polarisation, a new methodology was investigated in the case of ultrafiltration of fully retained protein solutions [17]. It relies on maintaining the wall concentration steady. However, this strategy seemed more adapted to filtration cut-off finer than microfiltration.

1.1.2. Flux

Considering the productivity aspect, maintaining a steady permeate flux is an efficient way to ensure the process productivity. However, the flux decreases as the fouling accumulates, which requires a TMP increase. The more the TMP increases, the more the wall deposit is compacted and consolidated and the more the filtration cake resistance to mass transfer increases. The flux reduces and the process selectivity is more altered [13].

1.1.3. TMP

Long term filtration processes undergo cake build-up and deposition which trigger enhanced TMP heterogeneity on the membrane length. In 1978, Sandblom patented a process aiming at solving this problem and premised the concept of uniform TMP filtration [18]. Vadi and Rizvi chose to control a process of skim milk microfiltration with this method [13]: they maintained a low and uniform TMP along the monolith, simultaneously insuring a high tangential fluid flow. This control permitted to obtain a steadier flux. The uniformity of the deposit on the monolith length and the stability of the process performance, linked to the product quality, were improved. At all cross flow velocities studied, the internal fouling was more significant under constant flux mode rather than under constant TMP mode [19]. The comparison between constant TMP mode and constant permeate flux mode of control led to the conclusion of a better performance for the first strategy. The uniform-TMP mode exhibits a lower initial flux than classical operation at the same tangential fluid velocity, but with time flux decline is significantly lower [19]. For all these reasons, the TMP appears as the best control parameter for improving the microfiltration process run. It was indeed the topic of many current research works and two membrane manufacturers have recently developed prototypes laying on the concept of uniform TMP filtration mode.

2. The existent uniform-TMP membranes

The PALL-EXEKIA company modified the membrane structure in order to develop a process operating at constant TMP [20]. The patented membrane Membralox GP® is characterized by a porosity gradient in its porous support layer. Its porosity radial increases beyond the active layer, so as to exert an additional counter-pressure in the direction of the permeate flow. It decreases longitudinally to create a permeability gradient in the direction of the treated fluid flow. This gradient approximately equals the pressure longitudinal gradient of the fluid in the membrane channel. The value of the transversal pressure drop was thus previously adapted to the tangential flow rate and the characteristics of the fluid viscosity. This results in a transversal pressure drop on both sides of the active surface, which is constant on the membrane length. Though this process permits to modify the porous support structure only, it presents the drawback of locally decreasing the support porosity and enhancing the accumulation of fouling during filtration. Moreover, this deposit is hardly swept during the cleaning step. This phenomenon may cause long-term fouling in the porous support. Otherwise, the porosity gradient may form highly heterogeneous fouling in the porous support. The permeate flow may be curbed to preferential hydraulic pathways, leading to heterogeneous permeate flux distribution and production along the membrane length.

With the purpose of solving this problem, the TAMI Company patented a new membrane prototype [21]. The active surface of this membrane was characterized by a thickness gradient decreasing toward the filtered fluid flow. This membrane permits to obtain a permeate flux constant along the membrane channels, since the active surface thickness varies proportionally to the pressure drop decrease. This thickness gradient is sized according to the pressure gradient between the membrane inlet and the membrane outlet, therefore determined by the chosen tangential fluid velocity [21]. However, the structure of the active surface is modified, which involves a more complex manufacturing.

This study aims to design a new membrane structure, intended to the filtration of highly fouling fluids, with the goal of improving the current efficiency of this filtration process. The idea was to develop a membrane prototype operating at a TMP as low and uniform as possible, so as to hinder the permeate flow inside the porous membrane support, and consequently limit fouling at the membrane surface and inside the membrane porous structure. This permits to maintain constant the qualitative and quantitative filtration properties. The applied methodology is both a modelling and an experimental approach.

Milk was chosen as the experimental fouling fluid. Modelling milk filtration remains difficult due to concentration polarisation and fouling, the sequence of those phenomena in the hydrodynamic description of the process and the complexity of this fluid structure. A preliminary hydrodynamic study was achieved by numerically modelling water filtration. This method enabled to approach solutions for the prototype design. By coupling this simulation work to experimental campaigns, the numerical model was first validated, and then completed with experimental results related to concentration polarisation and fouling.

3. Materials and methods

3.1. Designed monolith: principle and structure

The membrane used was a ceramic Kerasep^{TM} membrane (NOVASEP Applexion SAS, Saint Maurice de Beynost, France) with 19 channels and 0.1 μm average pore diameter, in a composite filtering layer of ZrO_2 on an alumina support (hydraulic diameter $d_h = 3.5$ mm, length $L = 1.18$ m, membrane surface $S = 0.256\ m^2$). A waterproof coating is laid on the external surface of the ceramic membrane, i.e., on the permeate side. This layer is only abraded on small surfaces, on the entire membrane circumference, using a conventional turning and milling machine. Those surfaces are called permeation vents and they constitute the pathway where permeate is collected. Applying this coating on the external layer modifies the counter-pressure on the permeate side. At the permeation vents, TMP varies and reaches maximal values that control the membrane production. This TMP variation at the vent location may also generate local flow destabilization favourable to mass transfer. Though coating limits permeation, it hinders the fouling build-up and it permits a more sustainable long-term production. The TMP in the membrane is lower than in classical membrane structure and the tangential velocity may simultaneously be maintained high. Considering the largest part of the monolith, on waterproof areas, TMP is constant and low. Therefore, a more uniform filtration cake is expected, leading to a better control of the process selectivity. Fig. 1 represents the scheme of the investigated structure. With the view of a longitudinal membrane section, the associated TMP profile is brought into line.

Width, number and position of the abraded vents describe the membrane configuration and were the parameters retained for the modelling study to achieve the prototype sizing. Those parameters

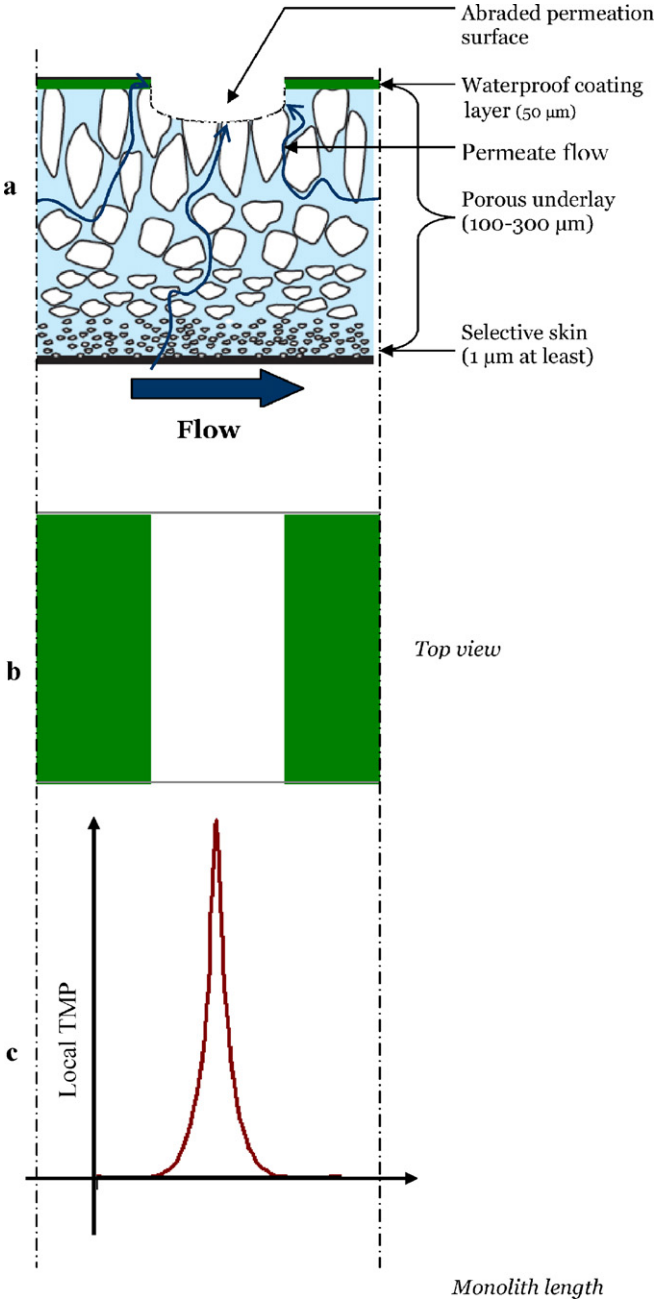

Fig. 1. Schematic principle of the flow in the designed membrane prototype: longitudinal section (a), monolith part top view (b) and associated pressure profile (c).

were optimized by studying their influence on the filtration performance, with the objective to reach the targeted permeate volume and quality. The targeted permeate flux for milk filtration was set at $100\ L\,h^{-1}\,m^{-2}$ at VCR = 1, under a TMP of 1 bar. Industrially, this value is the common standard for this protein separation process. Exhaustively, a casein-free permeate, characterized by a protein content superior to $4.5\ g\,L^{-1}$, fulfil the industrial constraints.

3.2. Mathematical model and performance criteria

The commercial software Fluent was used to simulate the fluid flow in the membrane. The mathematical model aims at solving the Darcy equation for a steady, laminar and three-dimensional flow. The basic conditions imposed to the flow were the following ones:

- the feed pressure along the membrane is the same whatever the channel considered, on a given monolith section and at a similar location
- the pressure drop between the channels is unimportant on a given cross section of the monolith
- the effects of the capillary and gravitational forces are negligible compared to the linear pressure drop in the membrane.

The Darcy law defines the membrane permeability (K) and links the fluid dynamic viscosity μ flowing through the active surface to the volume filtration flux (J) and the pressure drop at the membrane interface (ΔP):

$$J = \frac{K}{\mu}\Delta P \tag{2}$$

The flow was assumed isothermal and the porous support isotropic. The fluid was incompressible and Newtonian. In this case, the permeate flow expression was decomposed as follows:

$$u' = -\frac{k}{\mu}\frac{\partial P}{\partial x} \tag{3}$$

$$v' = -\frac{k}{\mu}\frac{\partial P}{\partial y} \tag{4}$$

$$w' = -\frac{k}{\mu}\frac{\partial P}{\partial z} \tag{5}$$

The continuity equation for an incompressible permeate flow was written:

$$\frac{\partial u'}{\partial x} + \frac{\partial v'}{\partial y} + \frac{\partial w'}{\partial z} = 0 \tag{6}$$

By combining those two previous equations, the following equation was obtained:

$$\frac{\partial^2 P}{\partial^2 x} + \frac{\partial^2 P}{\partial^2 y} + \frac{\partial^2 P}{\partial^2 z} = 0 \tag{7}$$

The value of k defines the porous layer. The boundary conditions imposed to the flow were:

- on the lateral surface and on the inlet and outlet membrane cross sections, the pressure was described by the equation:

$$\frac{\partial P}{\partial \boldsymbol{n}} = 0 \tag{8}$$

- at the permeation vent outlet, the permeate pressure was similar to the external pressure (equal to the atmospheric pressure or the pressure in the membrane module):

$$P = P_{\text{ext}} \tag{9}$$

- inside each channel, the following equation was verified:

$$-\frac{k}{\mu}\frac{\partial P}{\partial \boldsymbol{n}} = \frac{K}{\mu}(\text{TMP}) \tag{10}$$

with $\boldsymbol{n}$ the vector normal to the flow. This boundary condition defines the active layer. A no-flow boundary condition is imposed on the impermeable coating.

The decreasing pressure in membrane channels was linear with membrane length, according to the Hagen–Poiseuille law. This assessment is valid only under the assumption that the permeate flux is much lower than the feed flow, which was validated here. For this modelling work, the properties of pure water were considered for the feed flow. The membrane walls were assumed rigid and characterized by a constant permeability on the whole active surface. The accuracy of modelling results is principally based on the mesh accuracy designed to describe the flow precisely on each cross section of the monolith. The validation of grid independency was

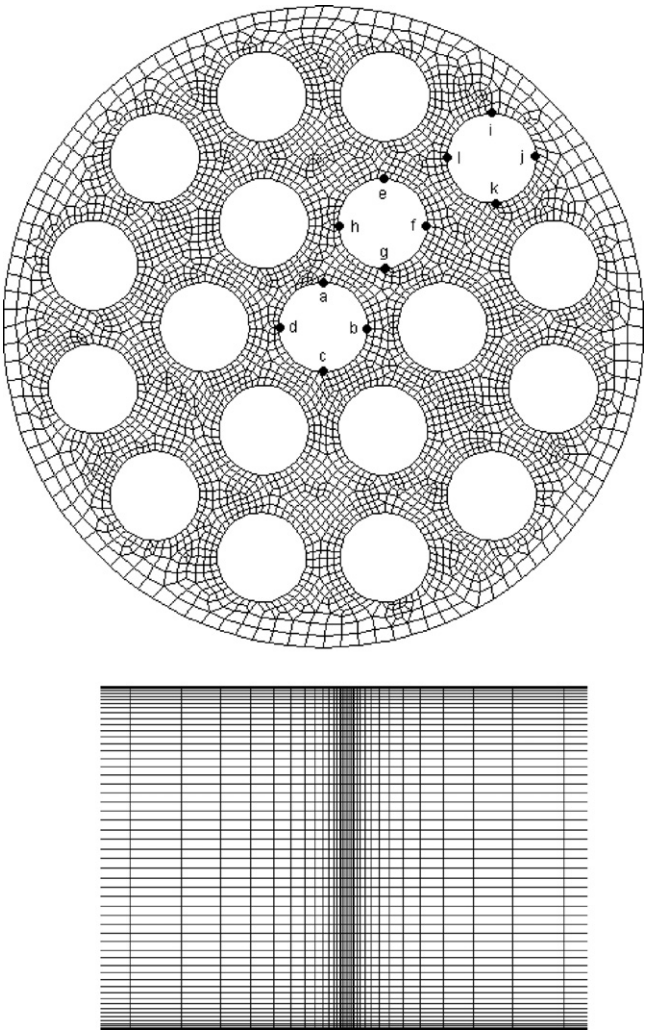

Fig. 2. Mesh used for the cross section (left view) and the lateral section (right view) of the membrane and simulation points.

validated by performing numerical simulation with varying number of nodes. The original grid has been refined twice by adding 25 and 50% of the cell number in every direction, mainly on the vent locations. Simulation results showed that there was no difference (less than 1%) in the pressure field over the monolith. Fig. 2 represents the final elaborated mesh. Each transverse section includes 1326 volumes and the 12 representative points designated from a to l are also shown. They are located on each channel corona and on several channel areas selected for this study. Considering the pressure gradient in the porous support those various points were positioned around each channel, with a 90° space between each point. The coating is located around the represented cross section and hence constitutes the circle perimeter (Fig. 2 Top)

Finally, three distinct structures were regarded in the modelling work. They were described with three different permeability values, experimentally determined:

- the skin, or the membrane active layer
- the porous medium
- the external coating delineating the waterproof areas of the membrane.

To calculate the ratio (J/τ_w), the wall shear stress was described with Eq. (11) [22]:

$$\tau_w = \frac{f}{2}\rho_r v^2 \tag{11}$$

where f is the wall friction factor, ρ_r is the density of the retentate, and v is the tangential flow velocity.

The friction factor was determined with the approximation of Drew in turbulent flow:

$$\frac{f}{2} = 0.0007 + 0.0625Re^{-0.32} \quad (12)$$

with Re the Reynolds number. This correlation is valid in a cylindrical straight tube for a turbulent flow and Newtonian fluid, with a wide range of validity $3000 < Re < 3.10^6$ [22].

The pressure profiles were calculated immediately downstream the active surface. TMP was obtained by subtracting the local pressure after the active surface to the pressure value in the membrane core. From those values, the TMP profiles were plotted on a two-dimensional figure either in the transverse or the radial section. The associated production fluxes were also calculated. The permeability of the uncoated zones being constant, the global flux provided by each vent was deduced from the modelling results. The permeability calculation is normalized with the total membrane active surface.

The numerical simulations in this work refer to the characteristics of a Kerasep® membrane (19 channels, 0.1 μm nominal pore size, 1.18 m length). Its active layer hydraulic permeability was set at 1250 L h^{-1} m^{-2} bar^{-1} and the membrane porous support permeability (k) 8750 L h^{-1} m^{-2} bar^{-1}. By default, for tangential filtration experiments, the inlet and outlet pressure values were, respectively in the range of: P_i = [2.2–2.7] bar and P_o = [0.5–1.0] bar, being equivalent to a global TMP of 1.35 bar and a tangential fluid velocity of 5 m s^{-1}. Results similar to literature were obtained [8,11,12,23,24].

The TMP profiles were compared altogether, on the basis of three criteria: the resulting membrane permeability, the TMP uniformity and the TMP stability. The uniformity of the TMP curves is illustrated by the standard deviation σ of the TMP.

$$\sigma = \sqrt{\frac{\sum_{i=1,n} (\mathrm{TMP}_i - \mathrm{TMP})^2}{n-1}} \quad (13)$$

The lower the calculated standard deviation, the more uniform the associated pressure profile.

The stability of the TMP profiles was defined because the standard deviation does not rigorously make the distinction between a TMP profile with all points slightly different from the average pressure and a TMP profile with most of simulation points close to this average value and only a few points extremely diverging. This second criterion is calculated as the absolute sum of the discrepancy of the pressure values between two consecutive points, balanced by the distance between them.

$$\zeta = \sum_{i=1}^{n} \frac{\left|\mathrm{TMP}_{i+1} - \mathrm{TMP}_i\right|}{(z_{i+1} - z_i)} \quad (14)$$

The lower the ζ value, the more satisfactory the pressure profile. The permeability associated to each membrane configuration was also calculated. This set of parameters permitted to evaluate the efficiency of the designed membrane.

3.3. Experimental device

The bench-scale microfiltration unit used is represented in Fig. 3. The tank, with a capacity of 100 L, maintains the fluid temperature constant throughout the experiments with a double-coated heat exchanger. The regulation was ensured by an automatic valve (Lucifer 481865A2). The flow circulation in the pilot loop was made by a feed pump (Leroy Somer LS100 LT). The pressure was measured by sensors (Bourdon Haenni Instruments, Croissy Beaubourg, France) to control the TMP. The temperature and the total feed flow in the unit loop were, respectively given by a temperature sensor at the (TI) measurement point and by a flowmeter Krohne IFC 010D (FI). The experiments were all performed in a recirculation mode, i.e., the permeate and the retentate recycled in the feed tank (VCR = 1). The chosen filtration process was the separation of the casein micelles from the skim milk bulk, soluble proteins, also called lactoserum proteins.

Table 1
Mean composition of the Marguerite® milk.

Compound	Concentration (g L^{-1})
Fat compounds	0.5
Proteins	30–36
of which casein micelles	24–28
Soluble proteins	6–8
Inorganic matter	9
of which linked to proteins	4
Lactose	50

The skimmed milk used for the experiments was the Marguerite® milk (Union des Coopératives Laitières de Villefranche (69400 Arnas, France)). Its average composition is given in Table 1.

During milk experiments, the TMP was raised progressively, with an increase of 0.4 bar every 20 min. At each TMP value performed, the stabilized mass flow rate was achieved. Filtration time necessary to reach steady flux conditions was preliminary determined and set at 25 min.

The membrane permeability was experimentally calculated as follows:

$$L_p = \frac{Q_p}{S \times \mathrm{TMP}} \times \frac{\mu(T)}{\mu_{20\ ^\circ\mathrm{C}}} \quad (15)$$

The experimental flux was calculated by agreement at a temperature of 20 °C for water and 50 °C for milk. The measured fluxes and permeabilities were normalized to the total membrane active surface.

At the end of filtration experiments, the cleaning step was performed. The regeneration of the membrane was carried out using the following protocol:

- rinsing with deionised water, at high temperature (60 °C, 20 min),
- basic washing with Ultrasil 25® (Henkel-Ecolab, SNC, Issy-les-Moulineaux, France) (0.5 wt.%) in which bleach is added with the same concentration. A flush is first performed during 30 min, with the permeate valve closed (TMP = 0.4 bar, v = 7 m s^{-1}, 60 °C), then the permeation runs 30 min longer (TMP = 1.9 bar, v = 7 m s^{-1}, 60 °C),
- rinsing with deionised water,
- washing with nitric acid (0.5 wt.%) or Ultrasil 75® (Henkel-Ecolab, SNC, Issy-les-Moulineaux, France) at the same concentration and at a temperature of 60 °C for half an hour (TMP = 1.9 bar, 60 °C, 20 min),
- careful rinsing with deionised water until pilot neutralization.

The evaluation of the permeate quality was achieved by measuring the total protein content in the samples using the Kjeldhal method and by checking the permeate clarity with the measurement of the turbidity at 20 °C (Turbidimetre Turb 550 IR, ISO 7027/DIN 27027). Casein micelles are strong colouring proteins, with a white and opaque coloration. The permeate opaqueness is therefore an indication of its protein concentration and it attests of a high micelle casein content. Transparency indicates a casein-free permeate. The calibration of turbidity versus casein micelle concentration in a translucent permeate was previously made. The obtained correlation was linear and it permitted to calculate the casein micelle content from the turbidity measurement of the col-

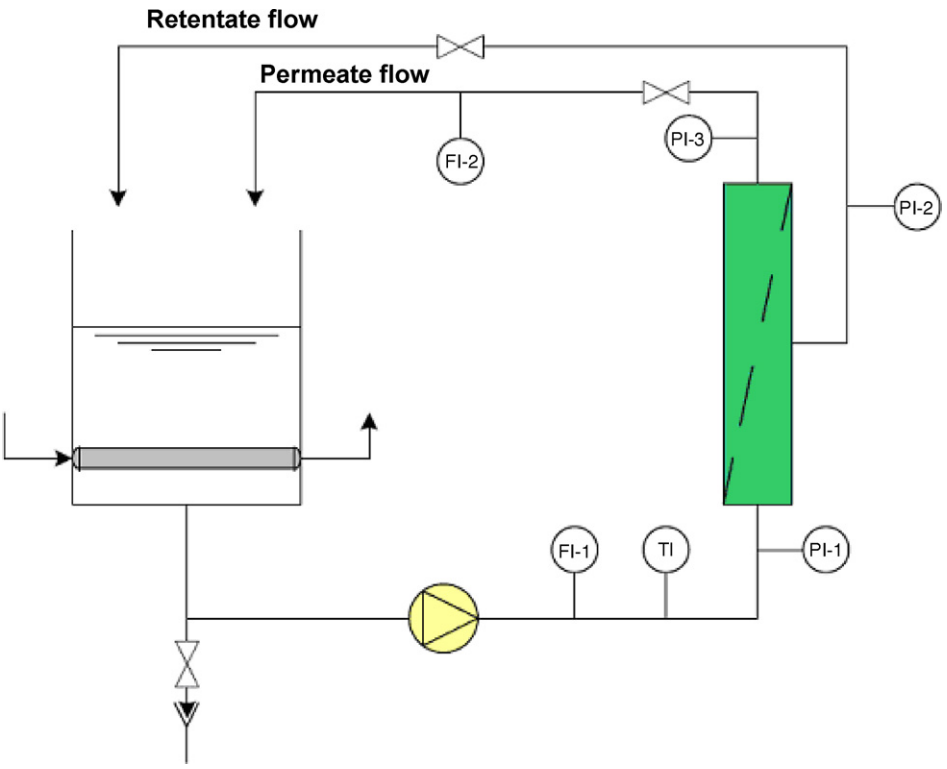

Fig. 3. Bench-scale filtration pilot plant.

lected samples. This estimation of the permeate quality was widely used in literature [25].

Combining the two analysis enabled to conclude about the permeate quality.

4. Results and discussion

The raw simulation results permit to obtain the local TMP variation according to the channel section for different flow velocities and simulated points. A study of the pressure characteristics was achieved versus the location of the simulated point inside a channel and versus the channel location in the membrane. The comparison of the pressure profiles inside a membrane channel revealed that most extreme TMP values were obtained for the simulated points taken the nearest to the membrane external surface. The results were similar if the comparison was drawn between similarly located simulation points in several channels. This means that permeate flow rates produced by the external channels are the highest. Therefore, the pressure profiles were considered at the modelled points i or j to examine the most significant TMP fluctuations.

The parameters that describe the membrane configuration, i.e., vent width and vent number, were investigated.

4.1. Influence of vent width on filtration

The considered configuration is a membrane with 8 vents homogeneously distributed along the monolith with respective distances from the membrane inlet of 147.5, 295.5, 443.5, 591.5, 739.5, 887.5, 1035.5 and 1145.5 mm. Fig. 4 represents the local TMP profiles along the monolith, plotted versus an increasing vent width [1–40 mm]. From 1 to 10 mm, the representative TMP characteristics coincide, which shows that a slight vent width variation has little repercussion on TMP profiles. Differences obviously appear between the curves of 10 and 40 mm. The TMP amplitude increases with the vent width, but in a moderate way. This finds explanation

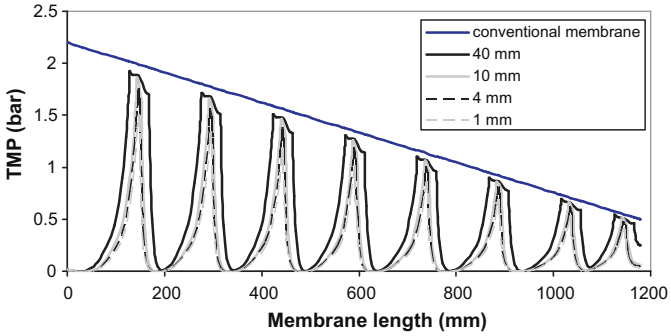

Fig. 4. Evolution of pressure profiles versus vent width [8 vents, i point, TMP = 1.35 bar, $v = 5\ m\ s^{-1}$].

in the fact that the permeate flux flowing through the active surface directly facing the vent is negligible in comparison with the permeate flux coming from the active surface located under waterproof coating. The increasing width of the vent also causes a deterioration of the pressure profile uniformity. Similarly, the stability of the pressure profiles is slightly modified and impaired.

Fig. 5 shows the permeability of all vents with width ranging from 1 to 40 mm. The permeability is normalized to the total filtration surface. Its characteristic is not linear and was not describable by any simple correlation. It sets into evidence that the relative benefits brought by an increasing size of the vents decrease when the initial vent size is high. Beyond a width of 8 mm, the curve can be correlated by a linear function. For a constant number of vents, it was possible to predict the width of vents to be abraded on the external surface of the monolith in order to achieve the industrial production figures. For instance, considering a permeability objective of $300\ L\ h^{-1}\ m^{-2}\ bar^{-1}$, the associated membrane configuration would comprise eight 25 mm-wide vents (Fig. 5). Adjusting the flux provided by each vent with its position data and its individual permeability on the monolith is also achievable.

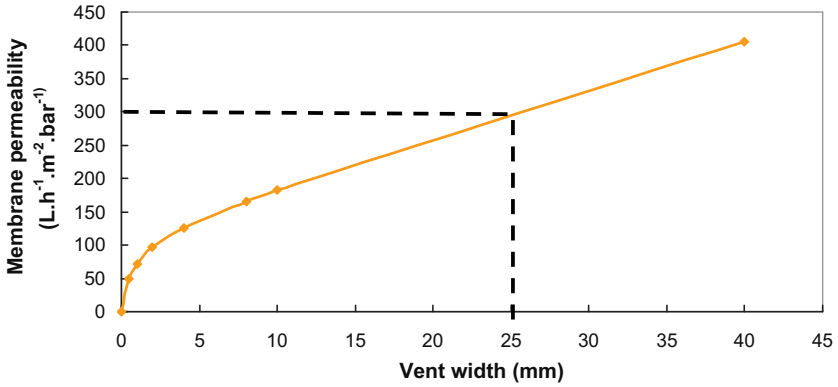

Fig. 5. Water permeability behaviour of the membrane comprising 8 vents of constant width, according to the vent width [i point, TMP = 1.35 bar, $v = 5\ m\ s^{-1}$].

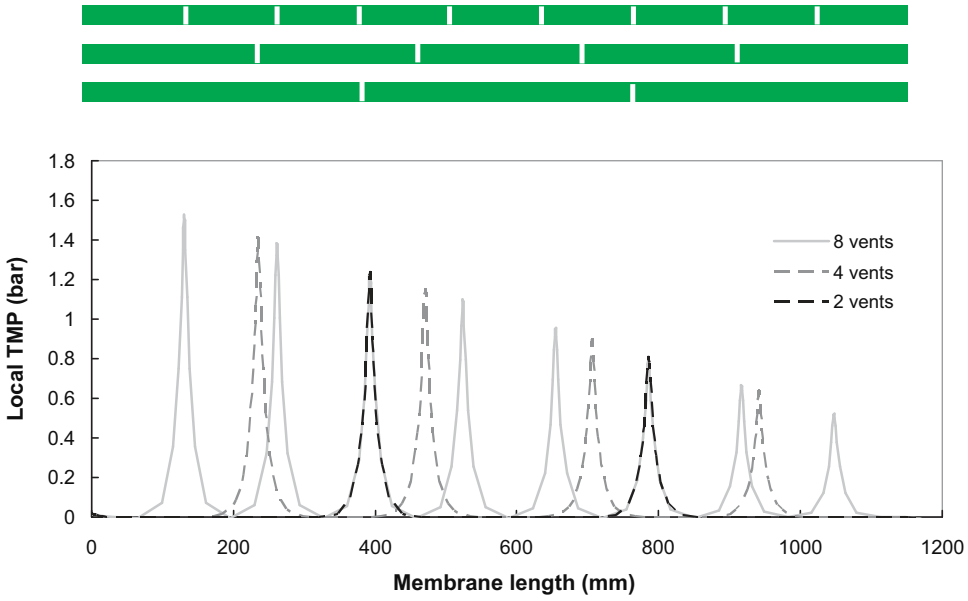

Fig. 6. Influence of the vent number on the local TMP profile and schematic of the associated monoliths [i point, TMP = 1.35 bar, $v = 5\ m\ s^{-1}$, width = 1 mm].

4.2. *Influence of vent number on filtration*

For these results, the width of vents was kept constant and equal to 1 mm. The vents were equally spaced on the membrane for each number, which means different locations depending on their number.

The number of vents abraded on the external surface of the monolith ranged from 1 to 40. When increasing the vent number, the first vents abraded on the monolith come closer to the membrane inlet. Therefore, the values of the local TMP applied to the first vents increase (Fig. 6). The calculation of the stability and the uniformity criteria showed that an increase of vent number barely deteriorates the uniformity of pressure profiles, but negatively influences their stability.

Concerning the hydraulic permeability of the membrane, for a number of vents taken between 0 and 20, a linear function linking the membrane permeability to the vent number was obtained (Fig. 7): $L_p = 9.13\ n$, where L_p is the total permeability of the monolith expressed in $L\ h^{-1}\ m^{-2}\ bar^{-1}$, and n is the number of vents. For a number of vents varying between 1 and 20, the production gain would be equal to the ratio of vent number increase. For instance, a configuration with 31 vents of 1 mm-width could be theoretically determined for a hydraulic permeability of $300\ L\ h^{-1}\ m^{-2}\ bar^{-1}$. The individual permeability of vents was calculated afterwards by taking into account the local TMP at each vent (Fig. 8). The individual vent permeability was almost steady for a number of vents ranging from 0 to 13 and diminished beyond this critical value. The production of each vent was therefore related to the total number of vents, which led to the notion of permeation interdependency. This phenomenon was mainly set into relief when filtering a highly fouling and concentrated fluid such as milk. When two contiguous vents were sufficiently spaced out, the TMP decreased to a null value on the membrane length between them. This meant the membrane skin, whose production depends on, was delineated.

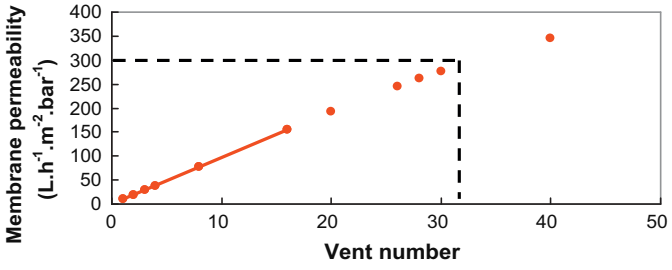

Fig. 7. Influence of the vent number, with an homogeneous distribution, on the monolith global permeability [TMP = 1.35 bar, $v = 5\ m\ s^{-1}$, width = 1 mm].

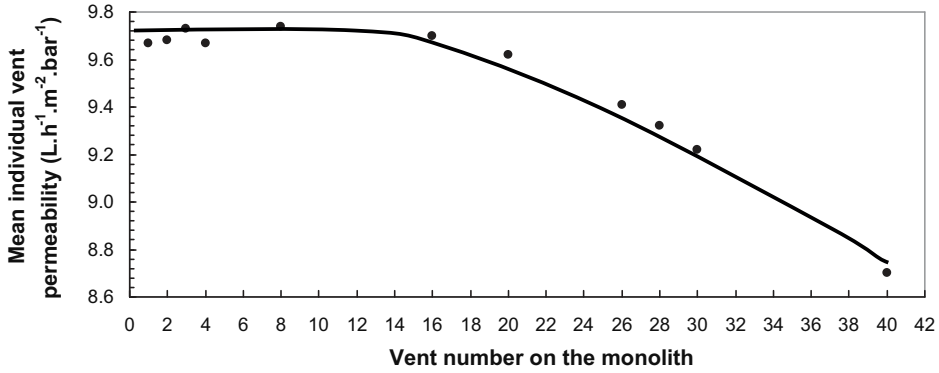

Fig. 8. Evolution of the average individual vent permeability as a function of the 1 mm-wide vent number. Correlation curve [TMP = 1.35 bar, $v = 5\ m\ s^{-1}$].

Table 2
Values of the maximal and minimal levels of the studied parameters involved in the modelling design.

Studied parameter	Level (−)	Level (+)
Vent width (mm)	1	40
Vent number	1	100
Cross-flow velocity ($m\ s^{-1}$)	5	6
Global TMP (bar)	1.35	3.85

Indeed, whatever the TMP considered for filtration, the membrane active surface involved in a 1 mm-wide vent permeation is equivalent to a length of 148 mm on the monolith (i.e., an active surface of $1.39 \times 10^{-3}\ m^2$ for each vent). For a different vent width, this equivalent length increases of as many mm as the permeation vent is widened.

If vents are moved closer, the same piece of active surface may contribute to permeate fluxes of consecutive vents. The permeation zones become connected and the vent production dependant. A minimal separation length for two consecutive vents was consequently defined to ensure an optimal permeability for each vent. From the modelling results, this critical value was rounded up at 80 mm. As far as possible, this separation length has to be respected for the prototype design.

4.3. Relative weight of the operating parameters

A modelling design was performed to investigate the influence of the process parameters on the filtration performance. This design aims at evaluating the relative influence of the parameters:

- related to the prototype geometry: vent number and vent width
- related to the process operating conditions: mean TMP and tangential fluid flow.

The impact of those four parameters on the permeate production, the stability and the uniformity of the pressure profiles was estimated by calculating the weight of each factor. The obtained weights were compared to each other, their absolute influence being properly impossible to quantify. The inferior and superior values of those factors are referenced in Table 2. Only one parameter at a time varied.

Table 3 synthesizes the effects of the investigated parameters on the membrane prototype properties and classifies them. An increase of vent number is more efficient than an increase of vent width to enhance the permeate flux. Increasing the vent width or the average TMP improved the uniformity and stability of the pressure profiles. Increasing the vent number enhanced the stability of the local TMP but slightly deteriorated the uniformity. Similarly, the tangential fluid flow had a positive impact on the monolith production but had a low or even null impact on the local TMP profiles. Indeed, the modelling studies were performed with water as model fluid, which excluded the involvement of fouling phenomena. This parameter would have been more influential if fouling phenomena had been taken into account. Finally, a TMP increase permitted to gain a proportional permeate flux, which would not be valid in the case of a fouling fluid such as milk. Similarly, increasing the vent width in the case of milk filtration would be irrelevant since it could enhance fouling in the porous support. When it comes to operating conditions, a compromise had to be found between the production optimum, the technological limitations for the prototype feasibility and the stumbling blocks related to fouling build-up, that were not considered in this work.

Table 3
Effect of the studied parameters on the prototype performance and parameters ranking.

Parameter	Effect		
	Flow	Uniformity	Stability
External surface permeability	++++	−	−
Vent width	++	0	−−
Vent number	+++	+	−−−
TMP	++++	0	−−−
Cross-flow velocity	+	0	0

+, positive impact; −, negative impact; 0, null.

The numerical modelling was thus an efficient and flexible tool to predict the membrane characteristics depending on the designed configuration and the operating conditions performed during the filtration. Lastly, it also provided predictive results, preliminary to an experimental study.

4.4. Experiments

Water experiments were performed with the purpose of validating the model used for numerical modelling.

A waterproof membrane was manufactured and a single 1 mm-wide vent was abraded 120 mm from the monolith inlet. The permeability of the complete waterproof coating was measured with deionised water and found equal to $1\ L\ h^{-1}\ m^{-2}\ bar^{-1}$ (Fig. 9). Two filtration directions were experimented. The circulation direction applying the lowest TMP to the vent is called «low TMP». In this case, the vent is located close to the membrane outlet, 1058 mm from the membrane inlet. Inversely for «high TMP», the considered vent is 120 mm from the membrane inlet. Similar results were obtained with a discrepancy of 3%. They were compared to the results obtained by numerical modelling (Fig. 9). A discrepancy percentage of about 5% was obtained, which enabled to corroborate the previous numerical results. Several other membranes were then coated and manufactured with various number

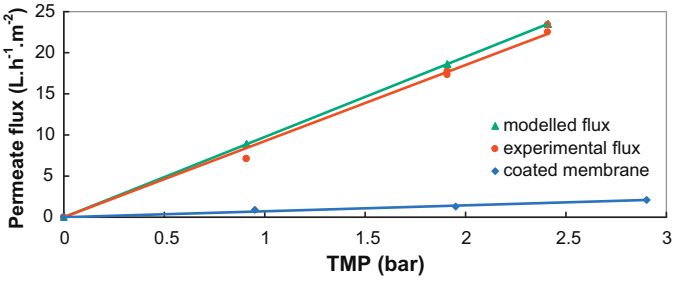

Fig. 9. Water permeate flux of one 1 mm-wide vent [dead-end filtration, 0.1 μm nominal pore size, 20 °C].

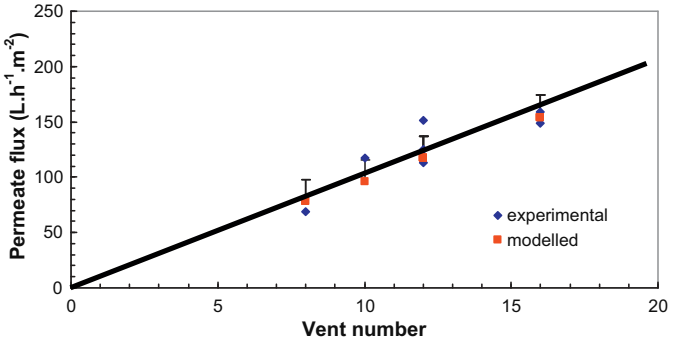

Fig. 10. Permeate flux as a function of the vent number for all the waterproof manufactured membranes and numerical predictions [dead-end filtration, 0.1 μm nominal pore size, 1 mm-wide vents, TMP = 1 bar, 20 °C].

of 1 mm-wide abraded vents, homogeneously distributed. Fig. 10 plots the associated permeability results for all those prototypes. The measurements were consistent to the numerical results, with a discrepancy inferior to the experimental error. It must be underlined that the permeability of an imperfect waterproof monolith was maximally evaluated at 20 $L\,h^{-1}\,m^{-2}\,bar^{-1}$, which explains why a few monoliths (standing for two experimental points) show higher permeability. Afterwards, prototype coating and manufacturing were optimized and a coated membrane permeability of 1 $L\,h^{-1}\,m^{-2}\,bar^{-1}$ was obtained in a reproducible way. In conclusion, the permeability values numerically determined were consistent with the experimental measurements, whatever the monolith configuration: number, width and position of vents. The constant flux of 2.3 $L\,h^{-1}\,bar^{-1}$ characterizes the hydraulic production of 1 mm-wide vent.

Milk filtration experiments were then performed. The permeate flux produced by one vent increased with the local TMP, in the range of [0.4–2.0] bar and its behaviour was rigorously reproducible for both filtration directions on the monolith (Fig. 11). Some monoliths

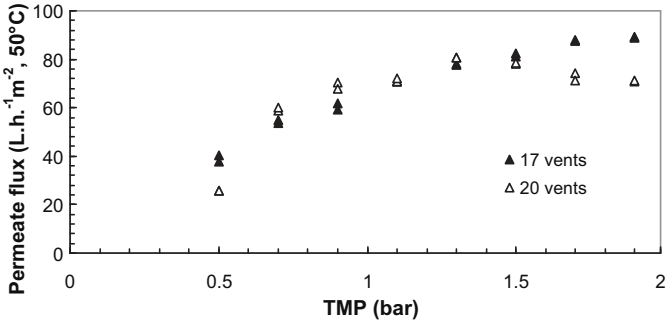

Fig. 12. Permeate flux variation with TMP for 17 and 20 vents of 1 mm width configurations during milk filtration [0.1 μm nominal pore size, $v = 6\,m\,s^{-1}$, 50 °C].

were then manufactured with various configurations. The influence of the vent number on quantitative production was first examined. The flux produced by a membrane is proportional to the number of vents abraded on its external surface, in the interval of [2–6] vents. This preliminary result is consistent with the results previously obtained with water. Fig. 12 compares the flux produced by two membranes with higher vent number, 17 and 20 vents of 1 mm width. Accounting for experimental discrepancy, the measured fluxes at increasing TMP were similar. For a vent number superior to 17, the permeate flux is not proportional to the vent number anymore. This result is consistent with the notion of minimal separation length previously established. For a vent number superior to 8, the minimal separation cannot be respected, and vent permeation interdependency is highlighted.

The vent width was also studied, in a range of width chosen to limit the fouling phenomena in the membrane porous support: 2.0, 1.0 and 0.5 mm. The measured permeate fluxes were found comparable with an experimental error of 5%. For simplicity and industrial feasibility, the width of 1 mm was chosen as the definitive width dimension.

Concerning the permeate quality, differences in the production behaviour were noticed. The permeate quality changed in accordance with the applied TMP: beyond a critical TMP ranging from 1.35 to 1.50 bar, the permeate became cloudy which means quality degradation (Fig. 13). To illustrate the sustainability of filtration characteristics with this membrane prototype, the ratio of permeate flux/shear stress was calculated for those experiments (Fig. 13). In Fig. 13 the critical value of the ratio permeate flux/shear stress, as established by Gésan-Guiziou et al., is symbolized by a horizontal line [10]. The experimental points were also positioned on this figure. It appears that under the TMP of 1.7 bar, the experimental points fit the empirical sustainable conditions set by Gésan-Guiziou et al. [10]. The permeate quality remained satisfactory. Above the TMP of 1.9 bar, casein micelle leakage was

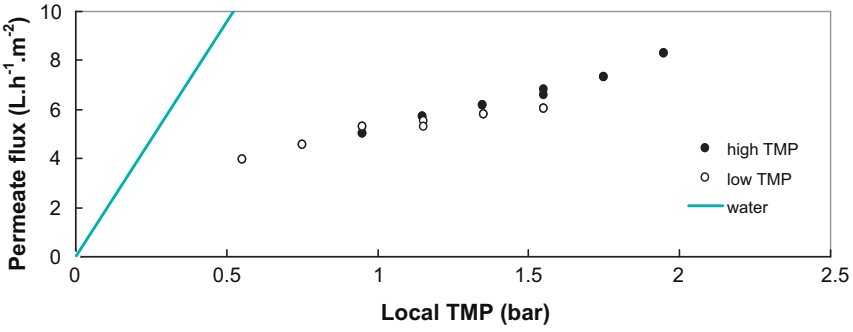

Fig. 11. Permeate flux versus TMP during Marguerite® milk cross-flow filtration with a single 1 mm-wide vent in the two filtration directions [0.1 μm nominal pore size, $L_{p0} = 10\,L\,h^{-1}\,m^{-2}\,bar^{-1}$, $v = 1.25\,m\,s^{-1}$, 50 °C].

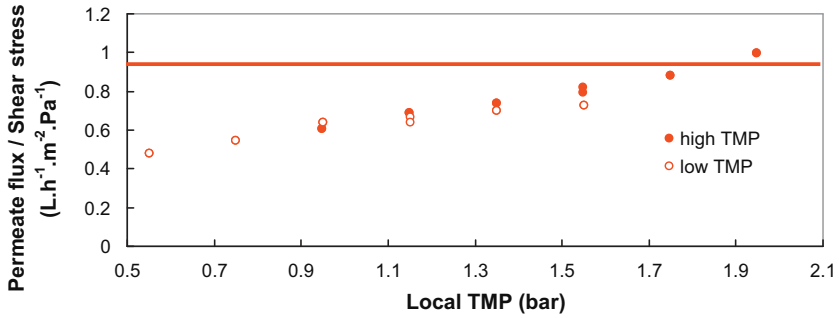

Fig. 13. Evolution of the ratio permeate flux/shear stress versus the local TMP [0.1 μm nominal pore size, $v = 1.25\ m\ s^{-1}$, 50 °C].

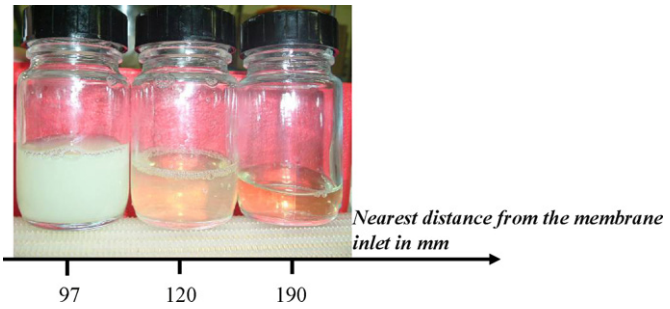

Fig. 14. Evolution of the permeate quality according to the location of the producing vent on the membrane [0.1 μm nominal pore size, TMP = 1.5 bar, $v = 1.25\ m\ s^{-1}$, 50 °C].

experimentally observed. The data points fall above the line, which confirms unsustainable operation. Considering the experimental discrepancy and the operating conditions of the experimental design (tangential fluid flow and filtration experimental device), the discrepancy between the work of Gésan-Guiziou et al. and those results were considered as satisfactory [10]. In addition to that, the permeate aspect strongly varied depending on the location of the studied vent and could be translucent or very opaque from the first instants of the filtration. Under sustainable operating conditions, opaque permeate was produced (Fig. 14) at the membrane inlet. The link between permeate quality and flow stabilization was done. The calculation of the length necessary to the steady state gave a value of 100 mm, which was consistent with experimental observations [26]. Lastly, permeate quality depends on operating conditions stability (TMP, temperature). In this case, some significant leaks of casein micelles that were observed could finally stabilize or disappear, as mentioned in some publications [4,10]. To conclude, the operating conditions, the vent location on the monolith and the TMP applied to the process are crucial factors for predicting the permeate quality.

For the design of the final prototype, experimental and numerical results were synthesized. No vent was placed in the unsteady state flow zones and beyond a local TMP of 1.5 bar. The membrane outlet will also be avoided due to the low local TMP that brings no significant benefits on the production. Finally, the collected permeate was produced by vents located on the central part of the monolith, homogeneously distributed on the available length. The final prototype configuration reaches a compromise between process operating conditions and qualitative and quantitative production:

- a high local pressure at the membrane inlet increases the permeate flux produced by all the vents but it moves further the flow developing length. The inlet membrane pressure may consequently be decreased in order to abrade more vents on the monolith. In this latter case, a possible counter permeation phenomenon must be considered. It may occur on the last centimetres of the monolith length if the membrane outlet pressure is too low;
- decreasing the tangential fluid flow allows bringing the inlet and outlet pressure values closer and thus make the vent permeation more uniform. However, a weak tangential fluid velocity enhances the fouling rate;
- increasing the vent number on the monolith length leads to an increasing global production. Even though, the separation distance between two consecutive vents has to be shortened, to the detriment of the independency of their permeation behaviour.

The final elaborated prototype comprises 17 vents of 1 mm and was designed to process an optimal TMP of 0.9 bar. This final configuration presents weakly uniform TMP, only by segments, on the monolith length. Its average TMP value is 0.4 bar, inferior to the classical membrane Kerasep™ and low on the major part of the active membrane surface (TMP < 0.4 bar is applied to more than 92% of the membrane skin), while the tangential flow velocity can be maintained high ($6\ m\ s^{-1}$).

Then, milk filtration experiments were launched with this prototype (Fig. 12). The permeate flux increases quasi linearly for TMP below 1 bar, which means that this critical TMP is the limit of reversible fouling conditions. Beyond 1.2 bar, the permeate flux stabilizes and the maximal permeate flux reaches $78\ L\ h^{-1}\ m^{-2}\ bar^{-1}$, 20% inferior to the initial objectives. Table 4 gathers the necessary data to evaluate the production quality. The produced permeate was translucent, therefore free from casein micelles. This observation was consistent with the turbidity measurements. The average total protein content shows fluctuations that depend on the process operating conditions and the filtration time. This protein content was measured about $4.5\ g\ L^{-1}$.

These characteristics were then compared to the filtration performance of a classical 0.1 μm nominal pore size ceramic membrane in the same operating conditions, industrially performed for this kind of protein separation. With a classical Kerasep™ filtration membrane, performance of milk filtration operation is not sustainable. Though the prototype and Kerasep™ fluxes were measured very close, both comprised between 70 and $80\ L\ h^{-1}\ m^{-2}$ for TMP [0.9–1.0] bar (Table 4), the process selectivity with Kerasep™ membrane was found irreproducible from one filtration to the other, and unsteady with the TMP increase. A critical pressure value was determined much inferior to 1 bar, above which occurs casein micelle leakage. The produced permeate is opaque (mean NTU value of 50.8), with a high concentration in casein micelles and a poor total protein content (Table 4). This implies performing the process at low TMP in order to maintain sustainable conditions, with the drawback of a weak production. Furthermore, the high pressure drop inside the membrane structure causes compacter fouling. Process selectivity is dramatically deteriorated. Indeed the protein content in the collected samples was rapidly

Table 4
Production characteristics with increasing TMP [0.1 μm nominal pore size, $v = 6\,m\,s^{-1}$, 50 °C].

	Optimal TMP (bar)	Production flux at this TMP ($L\,h^{-1}\,m^{-2}\,bar^{-1}$)	Permeate quality			
			Aspect	Mean turbidity (NTU)	Casein micelles content ($g\,L^{-1}$)	Total protein content ($g\,L^{-1}$)
Prototype	0.9	69–78	Limpid	6.3	0.0	4.17–4.86
Classical membrane	1.0	76	Opaque	50.8	0.3	3.4

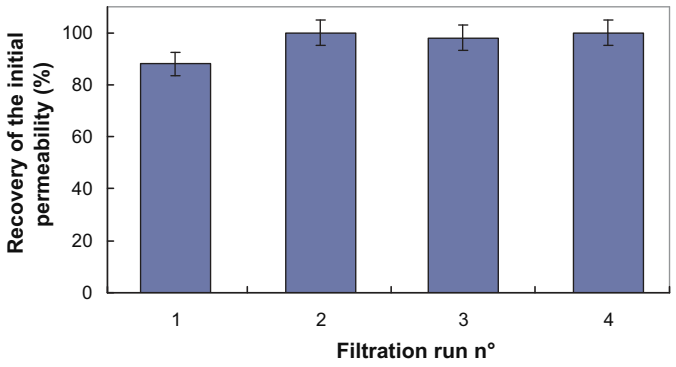

Fig. 15. Evolution of the membrane recovery evaluated on four consecutive filtrations and cleaning steps [prototype, 0.1 μm nominal pore size].

measured poor in lactoserum proteins. Last, the recovery of membrane permeability with a cleaning procedure achieves 80–90% of the initial membrane permeability, which demonstrates that irreversible fouling forms in the membrane porous support. This tends to diminish the subsequent process selectivity if the membrane is reused. Some filtered compounds are also retained in the tortuosity of the porous medium, while permeate flows to the membrane periphery. This assessment was confirmed by membrane autopsy.

The concept of our prototype structure was to add resistance to the flow and hinder the permeate circulation through the porous support. This could lower the cleaning efficiency and the assertion of an efficient cleaning of the resulting membrane is essential for filtration sustainability aspects, food safety and quality. The study of membrane permeability recovery when multiplying filtration runs was achieved. Fig. 15 represents the membrane cleanliness recovery after each filtration step ended with a cleaning step (according to the cleaning sequence listed in Section 3.3), on 4 consecutive filtration runs. Sequences of experiments were performed: permeability values were measured at the end of the cleaning protocol following the filtration run, and depicted in Fig. 15. Those figures show the membrane recovery expressed as the percentage of the initial membrane permeability. The results are satisfactory, with a membrane permeability recovery always higher than 90%.

5. Conclusion

In order to achieve a uniform TMP filtration process, the purpose of this study was to manufacture a new membrane prototype by modifying the classical structure of a ceramic tubular microfiltration monolith. When applying a waterproof coating on the external monolith surface, the dramatic TMP decrease induced by permeation at the membrane entrance was avoided. On the waterproof membrane parts, that represent the largest membrane external surface, the TMP is constant and low. Production control is induced by permeation vents. A more uniform TMP profile is ensured on the largest part of the monolith. The hydrodynamic aspect and the local TMP profiles of this prototype were investigated by numerical modelling. The modelling tool appeared as an efficient, flexible and easy-to-use tool to predict the process performance only with water. The limiting factor for production was brought into light: the resistance to the flow induced by the waterproof coating was applied on the monolith external surface. Thus the objective of the prototype design was achieved.

The parametric study of the membrane characteristics permitted to conclude about the influence of the geometric configuration on the filtration performance:

- adding vents on the monolith induces no change in the uniformity of the pressure profiles, it brings a linear total flux increase but deteriorates the pressure stability. The dependence of the individual vent production to the total vent number was demonstrated and the notion of minimal separation length was introduced.
- increasing the width of the vents triggers a slight deterioration of the uniformity and stability of the pressure profiles. Increasing vent width brings a significant but non linear total membrane permeability gain.

The first experimental results were water flux measurements and they allowed to validate the accuracy of the numerical predictions. They constituted a basis for the production estimation during milk filtration. Several interface phenomena were investigated with milk filtration runs. The relation between permeate quality and cake filtration structure was highlighted. Parameters like TMP, filtration time and location on the monolith, were also underlined. Finally, a prototype was sized. The quality of the resulting production was steady and satisfactory. The permeate fluxes were reached 20% inferior to the initial objectives due to the dependency of the vent behaviour. The prototype does not yield a higher flux than the original module but it permits to reduce the fouling in long term experiments. The recovery of the membrane permeability was demonstrated satisfying with a classical cleaning procedure.

The efficiency of this development methodology can be used for other membranes or for other applications processing complex fluids. It permits to limit the manufacturing of test prototypes and the number of experiments, all the while understanding the hydrodynamic behaviour of the depicted membrane configurations.

Acknowledgment

This work was supported by Carnot STAR Institute.

Appendix A. Nomenclature

J	volume filtration flux ($m\,s^{-1}$)
f	wall friction factor (–)
k	membrane support specific permeability (m^2)
K	active surface permeability (m)
L_p	membrane permeability ($L\,h^{-1}\,m^{-2}\,bar^{-1}$)
L_{p0}	membrane permeability after coating ($L\,h^{-1}\,m^{-2}\,bar^{-1}$)
$\boldsymbol{n}$	vector normal to the flow
n	global number of points considered for simulation
P(u, v, w)	pressure field (bar or Pa)
P_i	pressure at the membrane module inlet (bar)

P_{ext} external pressure (atmospheric pressure or pressure in the membrane module) (bar)
P_o pressure at the membrane module outlet, on the retentate side (bar)
ΔP pressure drop at the membrane surface (Pa)
Q_p volume permeate flow ($L\,h^{-1}$)
Re Reynolds number (–)
S membrane surface (m^2)
T temperature (°C)
TMP_i local TransMembrane Pressure at the i simulation point location (bar or Pa)
u' permeate velocity component on the x axis ($m\,s^{-1}$)
v' permeate velocity component on the y axis ($m\,s^{-1}$)
v tangential fluid velocity ($m\,s^{-1}$)
w' permeate velocity component on the z axis ($m\,s^{-1}$)
z_i distance of the i simulation point from the monolith inlet (m)

Subscripts
NTU nephelometric turbidity unit
TMP TransMembrane Pressure (bar or Pa)
VCR volume concentration ratio

Greek letters
μ fluid dynamic viscosity (Pa s)
ρ_r retentate density
σ standard deviation
τ_w wall shear stress (Pa)
ζ stability criterion (–)

References

[1] M. Mercier-Bonin, G. Gésan-Guiziou, C. Fonade, Application of gas/liquid two-phase flows during crossflow microfiltration of skimmed milk under constant transmembrane pressure conditions, J. Membr. Sci. 218 (2003) 93–105.
[2] G. Jonsson, P.L. Johansen, W. Li, Influence of membrane fouling on ultrafiltration and microfiltration processes, in: Proceedings of CEE-Brazil Workshop on Membrane Separation Processes, Rio de Janeiro, Brazil, May, 1992.
[3] V. Chen, Performance of partially permeable microfiltration membranes under low fouling conditions, J. Membr. Sci. 147 (1998) 265–278.
[4] O. Le Berre, G. Daufin, Skimmilk crossflow microfiltration performance versus permeation flux to wall shear stress ratio, J. Membr. Sci. 117 (1996) 261–270.
[5] I.G. Wenten, Mechanisms and control of fouling in crossflow microfiltration, in: Article presented at the Filtration Society's 1994 Shuttle Award Meeting, March, 1995.
[6] L. Ding, O. Al-Akoum, A. Abraham, M. Jaffrin, Milk protein concentration by ultrafiltration with rotating disk modules, Desalination 144 (2002) 307–311.
[7] O. Al-Akoum, L.H. Ding, L.Y. Jaffri, Microfiltration and ultrafiltration of UHT skim milk with a vibrating membrane module, Sep. Purif. Technol. 28 (2002) 219–234.
[8] R. Moll, P. Moulin, D. Veyret, F. Charbit, Dean vortices applied to membrane process. Part II. Numerical approach, J. Membr. Sci. 288 (2007) 321–335.
[9] Q. Yang, J. Chen, F. Zhang, Membrane fouling control in a submerged membrane bioreactor with porous, flexible suspended carriers, Desalination 189 (2006) 292–302.
[10] G. Gésan-Guiziou, E. Boyaval, G. Daufin, Critical stability in crossflow microfiltration of skimmed milk: transition to irreversible deposition, J. Membr. Sci. 158 (1999) 211–222.
[11] R. Ghidossi, E. Carretier, D. Veyret, D. Dhaler, P. Moulin, Optimizing the compacity of ceramic membranes, J. Membr. Sci. 360 (2010) 483–492.
[12] F. Springer, R. Ghidossi, E. Carretier, D. Veyret, D. Dhaler, P. Moulin, Determination of the wall shear stress by numerical simulation: membrane process applications, Chem. Prod. Proc. Mod. 4 (2009), Article 5 (a).
[13] P.K. Vadi, S.S.H. Rizvi, Experimental evaluation of a uniform transmembrane pressure crossflow microfiltration unit for the concentration of micellar casein from skim milk, J. Membr. Sci. 189 (2001) 69–82.
[14] P. Boyaval, C. Lavenant, G. Gésan, G. Daufin, Transient and stationary operating conditions on performance of lactic acid bacteria crossflow microfiltration, Biotechnol. Bioeng. 49 (1995) 78–86.
[15] M.R. Mackley, N.E. Sherman, Crossflow cake filtration mechanisms and kinetics, Chem. Eng. Sci. 47 (1992) 3067–3084.
[16] N. Lawrence, S.E. Kentish, A.J. O'Connor, A.R. Barber, G.W. Stevens, Microfiltration of skim milk using polymeric membranes for casein concentrate manufacture, Sep. Purif. Technol. 60 (2008) 237–244.
[17] R. Van Reis, E.M. Goodrich, C.L. Yson, L.N. Frautschy, R. Whiteley, A.L. Zydney, Constant C_{wall} ultrafiltration process control, J. Membr. Sci. 130 (1997) 123–140.
[18] R.M. Sandblom, Filtering Process, US Patent N° 4,105,547. 1978.
[19] H.K. Vyas, R.J. Bennett, A.D. Marshall, Performance of crossflow microfiltration during constant transmembrane pressure and constant flux operations, Int. Dairy J. 12 (2002) 473–479.
[20] D. Garcera, E. Toujas, Support macroporeux à gradient de perméabilité et son procédé de fabrication, Brevet européen N° 0,870,534 1998.
[21] A. Grangeon, P. Lescoche, T. Fleischmann, B. Ruschel, Membrane pour filtration tangentielle et son procédé de fabrication, Brevet Français N° 2797198. 2001.
[22] P. Moulin, D. Veyret, F. Charbit, Dean vortices: comparison of numerical simulation of shear stress and improvement of mass transfer in membrane processes at low permeation fluxes, J. Membr. Sci. 183 (2001) 149–162.
[23] P. Dolecek, Mathematical modelling of permeate flow in multichannel ceramic membrane, J. Membr. Sci. 100 (1995) 111–119.
[24] P. Dolecek, J. Cakl, Permeate flow in hexagonal 19-channel inorganic membrane under filtration and backflush operating modes, J. Membr. Sci. 149 (1998) 171–179.
[25] G. Rice, A. Barber, A. O'Connor, G. Stevens, S. Kentish, Fouling of NF membranes by dairy ultrafiltration permeates, J. Membr. Sci. 330 (2009) 117–126.
[26] F. Springer, E. Carretier, D. Veyret, P. Moulin, Developing lengths in woven and helical hollow tubes for Dean vortices flows, Eng. Appl. Comput. Fluid Mech. 3 (2009(b)) 136–147.